Thermally activated plastic deformation of Si single crystals at temperatures above 1173K

Suzuki, Tubasa
Department of Materials Science and Engineering, Kyushu University

Tanaka, Masaki
Department of Materials, Kyushu University

Morikawa, Tatsuya
Department of Materials, Kyushu University

Fujise, Jun
Advanced Evaluation and Technology Development Department, SUMCO Corporation

他

出版情報：Japanese Journal of Applied Physics. 62, pp.021001-1-021001-8, 2023-02-09. 応用物理学会
バージョン：

OPEN ACCESS

Japanese Journal of Applied Physics **62**, 021001 (2023) **REGULAR PAPER**

https://doi.org/10.35848/1347-4065/acb2b9

Thermally activated plastic deformation of Si single crystals at temperatures above 1173 K

Tubasa Suzuki[1,2*], Masaki Tanaka[3], Tatsuya Morikawa[3], Jun Fujise[2], and Toshiaki Ono[2]

[1]Department of Materials Science and Engineering, Kyushu University, 744 Motooka, Nishi-ku, Fukuoka 819-0395, Japan
[2]Advanced Evaluation and Technology Development Department, SUMCO Corporation, Imari, Saga 849-4256, Japan
[3]Department of Materials, Kyushu University, 744 Motooka, Nishi-ku, Fukuoka 819-0395, Japan

*E-mail: tsubasa_suzuki@sumcosi.com

Received March 24, 2022; revised January 9, 2023; accepted January 12, 2023; published online February 9, 2023

The effect of high-temperature heat treatment during production on the mechanical property of Si wafer, namely yield stress, was studied through tensile tests of Si single crystals at 1123–1373 K, where stress–strain curves were obtained along the [$\bar{1}$34], [011], [001], and [$\bar{1}$11] directions. The critical resolved shear stress showed a remarkable temperature dependence, and it decreased with increasing test temperature. Below 1348 K, the activation enthalpy determined through strain rate jump tests showed no significant difference between crystals made by the Chokralski and the floating zone methods. This indicated that the solute oxygen does not influence the thermally activated dislocation glides. The activation enthalpy of 4.9 eV for a dislocation glide was much higher than that reported by previous studies (2.2 eV at temperatures below 1100 K), indicating that the thermal activation of dislocation glide is different from kink-pair nucleation. It was found that self-diffusion can assist the dislocation glide at temperatures above 1130 K.

1. Introduction

Dislocations introduced in Si wafers cause misalignment during nano-level fabrication due to plastic deformation. Moreover, they also cause unintended current leakage by acting as acceptors or donors, which reduces the manufacturing yield.[1–5] With the rapid development of semiconductor device manufacturing technology in recent years, circuit widths have become increasingly narrower and the defect control requirements for Si wafers have become more demanding.[6,7] Most of these dislocations are formed during heat treatment at high temperatures rather than during the machining process at room temperature, as Si crystals are brittle at room temperature. Dislocations are formed not only during the growth of single-crystal wafers but also by the large-scale integration (LSI) of devices. The phenomenon is particularly prominent in the shallow trench isolation (STI) process. The differences in the thermal expansion coefficients of the wafer and the nitride film deposited on it cause high stress on the film edge. This results in the generation of dislocations during the cooling stage after heat treatments.[8–10] In general-purpose {001} wafers, tensile stresses are usually applied in the direction parallel to the plate surface, such as the [011] direction.

The yield point phenomenon of Si is an important mechanical property. Many studies have been performed in the limited temperature range of 900–1100 K, which is the relevant range in the wafer fabrication process. It has been reported that the yield stress in the temperature range of 900–1100 K is strongly temperature-dependent.[11–18] With the development of Si wafer manufacturing technology, research on high-temperature heat treatment, such as rapid thermal processes in which wafers are rapidly heated above 1200 K for oxidation, has been actively conducted since the year 2000.[19–23] Thus, the demand for device processes at temperatures near or above 1200 K is increasing, and further understanding on the yield behavior of Si at these conditions is necessary.

Therefore, in this study, we aimed to elucidate the effects of temperature and oxygen content on yield stress through tensile tests and by comparing the results with that of previous studies.

2. Experimental methods

The tensile specimens used in this study were cut out from commercially available {111} and {001} silicon wafers. Figure 1 shows a schematic of the tensile specimen. The plane normal to the wafers was slightly tilted from the exact [111] and [001] directions, which is the so-called off-angle. To elucidate the dependence of the yield stress on the tensile orientation and temperature, tensile specimens with different initial tensile axes, such as [$\bar{1}$34], [011], [001], and [$\bar{1}$11], were prepared. The tensile axes were calculated from the notch and plane orientation of the wafer before cutting. The Si wafers were grown by the Chokralski (Cz) method, and the oxygen content of the solid solution was fixed at 2.4×10^{-3} mol%. To examine the effect of oxygen content, additional specimens were prepared by the floating zone (Fz) method, in which the oxygen content was less than 2.0×10^{-4} mol%. Due to the limited size and number of Fz wafers, only the [011] tensile specimens were prepared. Tensile tests were performed in a vacuum chamber with an oxygen partial pressure of approximately 10^{-6} Pa at an initial strain rate of 4.7×10^{-4} s^{-1} at temperatures between 1123 K and 1373 K. The tensile tests were recorded using a charge-coupled device (CCD) camera installed in the tensile machine (YONEKURA CATY-T3H). Strain was measured between two points separated by 2.0 mm on the specimen surface using software (DITECT, Dip-Motion). The yield point was defined either as the lower yield stress or as the 0.2% proof stress when the yield point phenomenon was not observed. After the yield point, a strain rate jump test was performed to measure the activation parameters. The strain rate after the rapid change was set at 4.7×10^{-3} s^{-1}, which was 10 times higher than the initial strain rate.

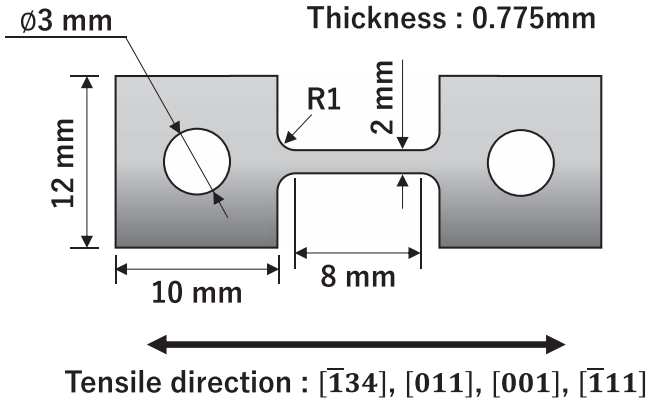

Fig. 1. Schematic illustration of a tensile specimen.

3. Results and discussion

3.1. Results

Figure 2 shows the stress–strain (s–s) curves, which were obtained up to a total nominal strain of 0.2 and where (a), (b), (c), and (d) correspond to the [$\bar{1}$34], [011], [001], and [$\bar{1}$11] tensile axes directions of Cz silicon, respectively. Figure 2(e) shows the s–s curves of Fz silicon along the [011] tensile axis. The yield point phenomenon was observed below 1300 K. The dislocation density increased abruptly in the low-temperature range at yielding, whereas it increased only gradually when the temperature was higher.[13] Figure 3 shows the relationship between the critical resolved shear stress (CRSS) and the test temperature. The yield stress was observed to decrease with an increase in the test temperature above 1,323 K. The yield stress of Fz wafers showed nearly the same temperature dependence with that of Cz wafers in the temperature range studied, which is consistent with the results of Sumino and Yonenaga.[14,24] The CRSS of the specimens with the [001] and [$\bar{1}$11] tensile axes were approximately 5 MPa higher than those of the specimens with the [$\bar{1}$34] and [011] tensile axes at all temperatures. This indicates that Schmid's law breaks down in the temperature range of 1173–1373 K. The details of this phenomenon will be discussed later.

In general, the temperature dependence of yield stress is explained using its two components, i.e. the effective stress and athermal stress. Here, the stress required for plastic deformation $\tau(T)$ at a certain temperature T is given by the following equation:[25]

$$\tau(T) = \tau_i + \tau^*(T, \dot{\gamma}), \tag{1}$$

where τ_i is the athermal stress, $\dot{\gamma}$ is the shear strain rate, and $\tau^*(T, \dot{\gamma})$ is the effective stress. Since the activation energy G^* is dependent on temperature and stress (in this case, the effective stress), its total derivative can be expressed as

$$\begin{aligned} dG^*(T, \tau^*) &= \left(\frac{\partial G^*}{\partial T}\right)_{\tau^*} dT + \left(\frac{\partial G^*}{\partial \tau^*}\right)_T d\tau^* \\ &\equiv -S^*(T)dT - V^*(\tau^*)d\tau^*, \end{aligned} \tag{2}$$

where S^* is the activation entropy, and V^* is the activation volume. $\dot{\gamma}$ is given in terms of the Burgers vector b, the number of dislocations N_0, the frequency factor ν, the Boltzmann constant k, and the area S_0 swept by a dislocation as[25]

$$\dot{\gamma} = bN_0S_0\nu \exp\left(-\frac{G^*}{kT}\right), \tag{3}$$

then

$$\begin{aligned} G^* &= -kTln(\dot{\gamma}/\dot{\gamma}_0) \\ &- kln(\dot{\gamma}/\dot{\gamma}_0) = G^*/T, \end{aligned}$$

where

$$\dot{\gamma}_0 = bN_0S_0\nu. \tag{4}$$

From Eqs. (1) and (2), the following can be asserted:

$$\begin{aligned} V^* &\equiv -\left(\frac{\partial G^*}{\partial \tau^*}\right)_T \\ &= kT\left\{\frac{\partial\, ln(\dot{\gamma}/\dot{\gamma}_0)}{\partial \tau^*}\right\}_T \\ &= kT\left\{\frac{\partial\, ln(\dot{\gamma}/\dot{\gamma}_0)}{\partial \tau}\right\}_T. \end{aligned} \tag{5}$$

If the flow stresses corresponding to two different strain rates γ_1 and γ_2 are τ_1 and τ_2, respectively, the activation volume can be written as[25]

$$V^* = kT\frac{ln(\dot{\gamma}_2/\dot{\gamma}_1)}{(\tau_2 - \tau_1)}. \tag{6}$$

Figure 4 shows the dependence of activation volume on the yield stress obtained by Eq. (6). Henceforth, we focus only on the [011] tensile direction, which is important during the device production process. The activation volume decreased with an increase in the yield stress. As shown by the black dotted line in Fig. 4, this trend was the same for both Cz and Fz. Through stress-relaxation tests, Omri et al. showed that the activation volume of Si was ~200 (b^3), which is ~800 (b^3) smaller than that obtained in the present study.[11] It is postulated that the thermal activation mechanism for dislocation glide is different in their study due to different test temperatures. This will also be further discussed later.

Partially differentiating both sides of Eq. (4) by $1/T$ gives

$$-k\left\{\frac{\partial ln(\dot{\gamma}/\dot{\gamma}_0)}{\partial(1/T)}\right\}_{\tau^*} = G^* + \frac{1}{T}\left\{\frac{\partial G^*}{\partial(1/T)}\right\}_{\tau^*}. \tag{7}$$

Additionally, Eq. (2) can also be written as

$$\begin{aligned} \left\{\frac{\partial G^*}{\partial(1/T)}\right\}_{\tau^*} &= -T^2\left(\frac{\partial G^*}{\partial T}\right)_{\tau^*} \\ &\equiv T^2S^*. \end{aligned} \tag{8}$$

Substituting Eqs. (8) into (7), the following can be obtained:

$$-k\left\{\frac{\partial ln(\dot{\gamma}/\dot{\gamma}_0)}{\partial(1/T)}\right\}_{\tau^*} = G^* + TS^* \equiv H^*, \tag{9}$$

where H^* is the activation enthalpy (apparent activation energy). By rewriting Eq. (9) using Eq. (5), the activation enthalpy can be formulated as[25]

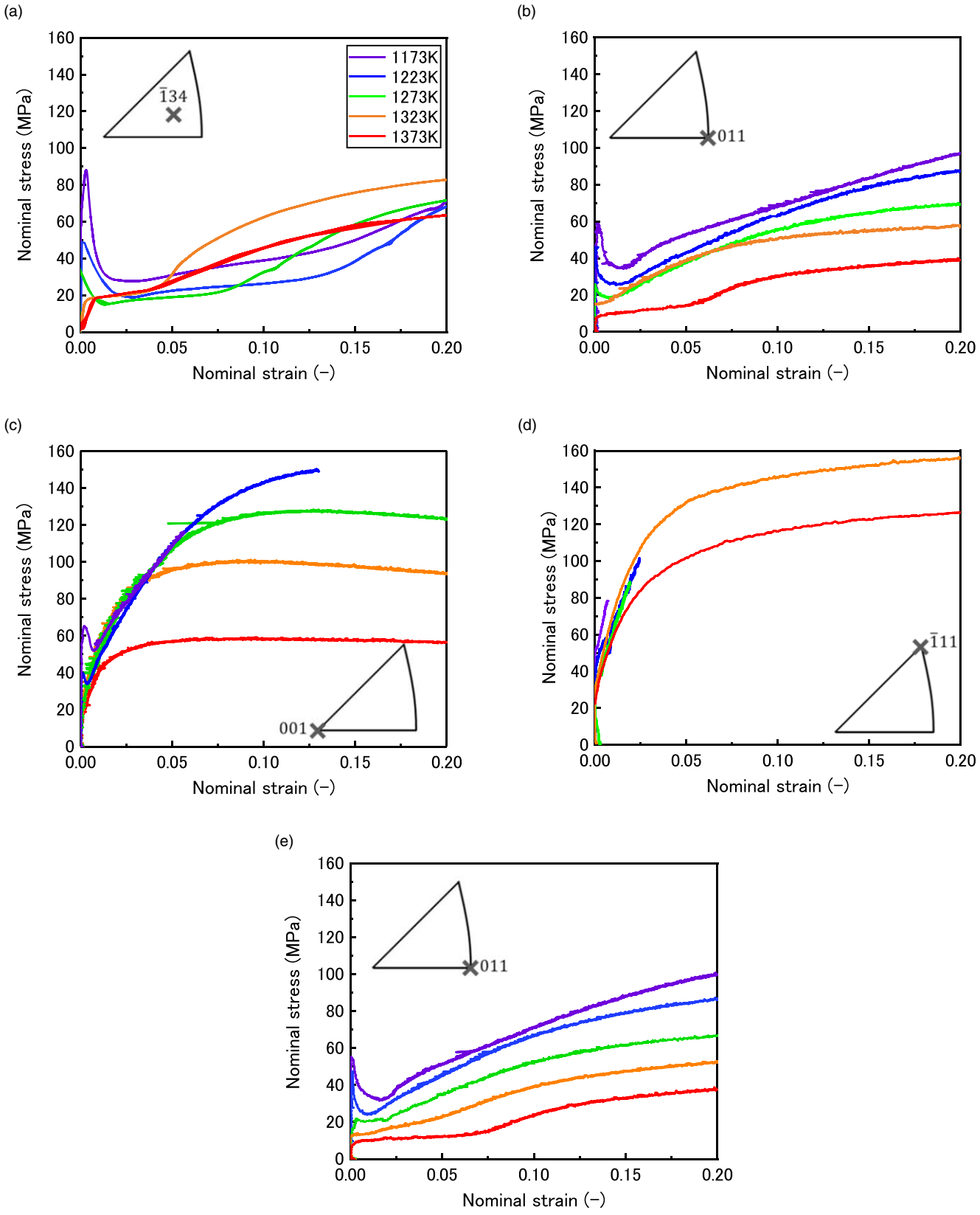

Fig. 2. (Color online) Stress–strain curves from the specimens tested at several temperatures. Tensile direction in the standard triangles are also shown in each figure. (a) Tensile direction is [$\bar{1}$34], (b) Tensile direction is [011], (c) Tensile direction is [001], (d) Tensile direction is [$\bar{1}$11] (e) Tensile direction is [011]. (a)–(d) Specimen is made from Cz wafer, (e) Fz wafer.

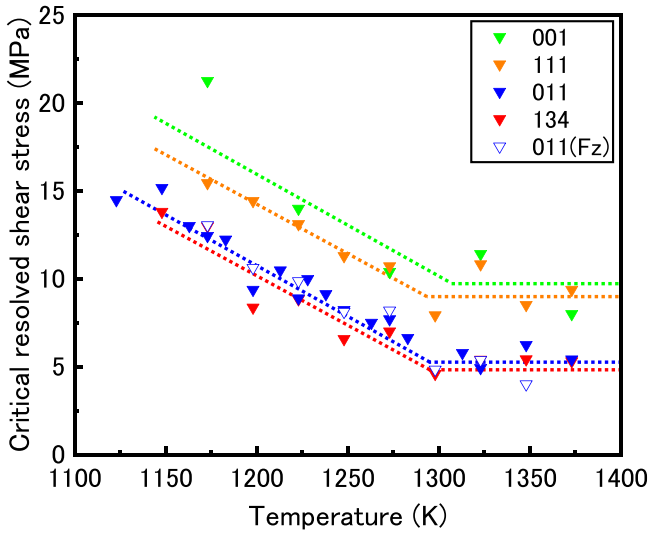

Fig. 3. (Color online) Relationship between the CRSS obtained from lower yield point and temperature. Filled plots indicate Cz, while unfilled plots indicate Fz results.

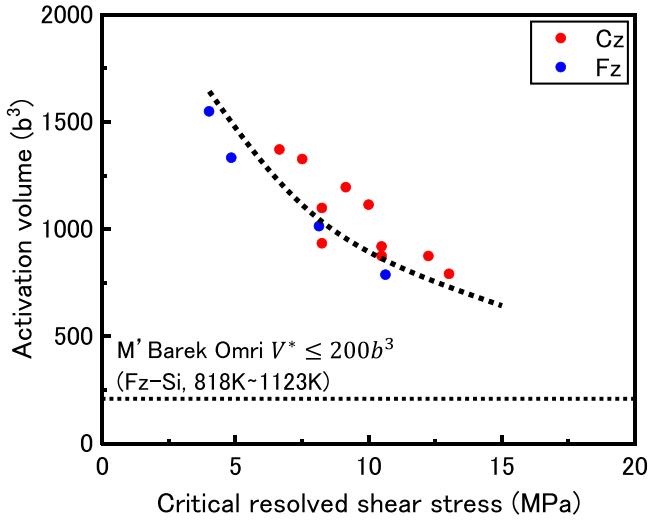

Fig. 4. (Color online) Relationship between activation volume and CRSS. The red plots show Cz and the blue plots show Fz, both coinciding on the same curve. The dotted line at the bottom of the figure shows the activation volume values obtained in a previous study by M' Barek Omri.[11)]

$$
\begin{aligned}
H^* &= -k\left\{\frac{\partial ln(\dot{\gamma}/\dot{\gamma}_0)}{\partial(1/T)}\right\}_{\tau^*} \\
&= kT^2\left\{\frac{\partial ln(\dot{\gamma}/\dot{\gamma}_0)}{\partial T}\right\}_{\tau^*} \\
&= -kT^2\left\{\frac{\partial ln(\dot{\gamma}/\dot{\gamma}_0)}{\partial \tau}\right\}_{T}\left(\frac{\partial \tau}{\partial T}\right)_{\dot{\gamma}} \\
&= -TV^*\left(\frac{\partial \tau}{\partial T}\right)_{\dot{\gamma}}. \qquad (10)
\end{aligned}
$$

The relationship between the test temperature and the activation enthalpy obtained from Eq. (10) is shown in Fig. 5. The blue dots in the figure are from the Fz wafers, and the red dots are from the Cz wafers. No apparent difference was observed in the values of the activation enthalpy from Fz and Cz. The average value of activation enthalpy was determined to be ~4.9 eV, which is about twice as large as that in a previous study (2.2 eV at low temperatures, dislocation-free

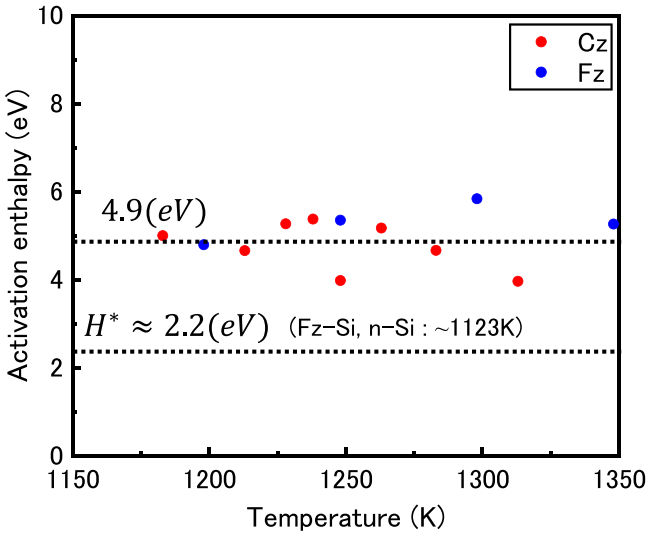

Fig. 5. (Color online) Temperature dependence of activation enthalpy. The red and blue plots show Cz and Fz, respectively, whose values are approximately 4.9 eV. The dotted line at the bottom of the figure shows the value of activation enthalpy of 2.2 eV at temperatures below 1123 K obtained in the previous study.[26,27)]

n-Si and Fz-Si).[26,27)] Although the margin of error was ~1 eV, it was observed not to vary significantly with temperature.

3.2. Discussion

3.2.1. Relation between dislocation core spread and Schmid's law. In this section, we first discuss the temperature dependence of the effective stress and dislocation motion. As shown in Fig. 3, the yield stress varies significantly along the different tensile axes, especially when the temperature is below 1,300 K. This implies that the CRSS is different along each tensile axis. If Schmid's law applied here, the CRSS would be constant regardless of the tensile axes for a given temperature and strain rate. Since this is not the case, Schmid's law does not seem to apply in the temperatures range of this study. Such a breakdown of Schmid's law has been reported for many bcc structures, where the Peierls stress is high.[28,29)]

Several hypotheses focusing on the core structure of screw dislocations have been proposed for such phenomena.[30–33)] Groger et al. performed simulations using bond order potentials and found that the screw dislocation core selectively extends parallel to the [110] plane upon application of a simple shear stress along this plane.[29,34)] In addition, Edogawa et al. performed theoretical calculations of the change in the potential for a screw dislocation to glide when a stress is applied. They showed that the potential field around the dislocation core changes with the direction and magnitude of the applied stress,[35)] which is due to the inhomogeneity of the Peierls potential. The results of this study suggest that such a mechanism also applies to Si. Considering that the potential field changes with the direction of applied stress, the dislocation core structure should also follow a similar trend.

Figure 6 shows the crystal structure of Si projected along the [110] direction, where the slip plane for a screw dislocation at the center of this figure would be $(1\bar{1}1)$ or $(\bar{1}11)$. If a shear stress is applied parallel to either the [001] or $[2\bar{2}1]$ direction, the screw dislocation should easily glide along the $(1\bar{1}1)$ plane following Schmid's law. However, the

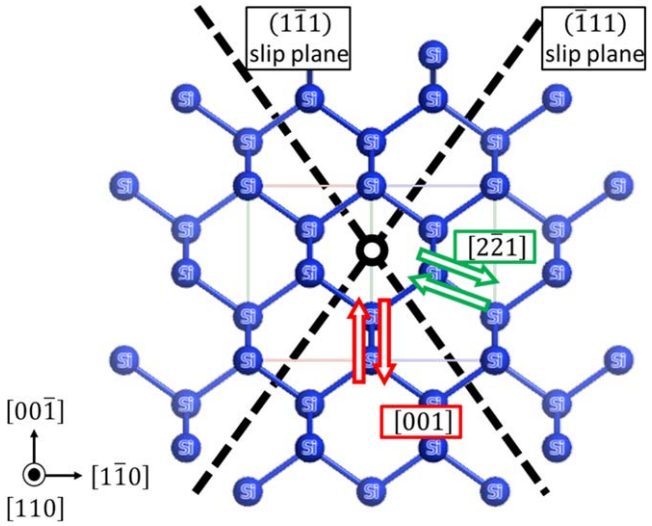

Fig. 6. (Color online) Model of dislocation core for a screw dislocation projected to the [110] plane in Si. The slip planes of [111] are indicated by dotted lines. The shear direction to move dislocation is indicated by a pair of arrows.

core of a screw dislocation dilatates inhomogeneously upon application of a shear stress in the present study, which leads to the breakdown of Schmid's law. Hence, further investigation on the change in the core structure using first-principles calculations is necessary.

3.2.2. Derivation of the activation energy for dislocation motion at low effective stress. As shown by Johnston, the yielding of crystalline materials is closely linked to the mobility and velocity of dislocations.[36] In Si single crystals, the barrier for dislocation motion is the Peierls potential.[37] In covalent crystals with a large Peierls potential, such as semiconductors, dislocation motion is governed by the formation and motion of kink pairs until the temperature where creep deformation is activated.[38–43] Numerous experimental studies have shown that the dislocation velocity v in semiconductors such as Si follows the empirical equation:

$$v = B_0\left(\frac{\tau^*}{\tau_0}\right)^m \exp\left(-\frac{H^*}{kT}\right), \tag{11}$$

where $\tau_0 = 1$ MPa and B_0, τ_0, and m are constants. From studies involving the deformation of Si at 900–1100 K, it is known that $H^* = 2.2$ eV and $m = 1.0$.[26,27] However, since the measurements of the activation enthalpy have only been performed in a narrow temperature range, its applicability to a wider range remains unclear.

Here, the strain rate $\dot{\gamma}$ is given by the following equation:

$$\dot{\gamma} = \rho b v = \rho b B_0\left(\frac{\tau_a - \tau_i}{\tau_0}\right)^m \exp\left(-\frac{H^*}{kT}\right), \tag{12}$$

where ρ is the mobile dislocation density, τ_a is the applied shear stress, and τ_i is the athermal shear stress. The effective shear stress τ^* is expressed as $\tau_a - \tau_i$. The magnitude of activation energy agrees well with Eq. (12) at most temperatures below 1100 K. However, the equation is multiplied by τ^* as a pre-factor, and the stress dependence of H^* has not been considered yet. In this section, we discuss whether theoretical equations can be used to derive the activation energy of dislocation motion when the effective stress is smaller than the Peierls stress.

Figure 7 schematically shows the variation in the activation energy with distance x when a dislocation overcomes a short-range obstacle, wherein L is the interval of the short-range obstacles. When an effective shear stress τ^* is applied and the activation energy G^* is obtained from the thermal vibration, the dislocation overcomes the short-range obstacle. Here, G^* is given by the following equation:

$$G^* = F - \tau^* V^* - TS^*, \tag{13}$$

where F is the Helmholtz free energy for dislocation motion. Assuming the entropy term to be negligible, the frequency p of this thermal activation process per unit time can be expressed as

$$p = \nu \exp\left(-\frac{F - \tau^* V^*}{kT}\right), \tag{14}$$

where ν is the vibrational frequency of the dislocation. The plastic shear strain γ can be expressed by the following equation:

$$\gamma = N_0 b S_0, \tag{15}$$

where N_0 is the number of dislocations. Equations (14) and (15) give the strain rate $\dot{\gamma}$ as

$$\begin{aligned}\dot{\gamma} &= \gamma p \\ &= N_0 b S_0 \nu \exp\left(-\frac{F - \tau^* V^*}{kT}\right).\end{aligned} \tag{16}$$

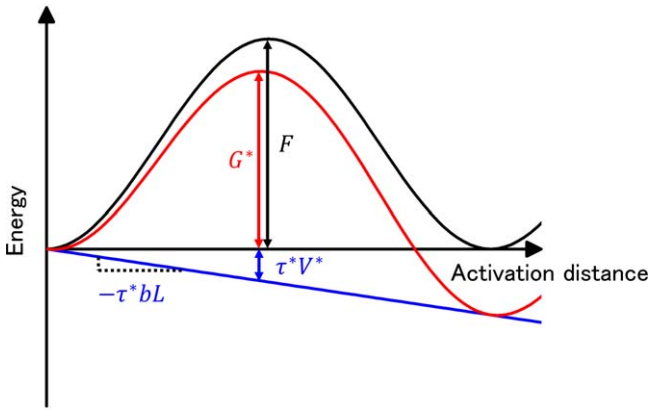

Fig. 7. (Color online) Relationship between energy and distance when a dislocation overcomes a short-range obstacle. F is the Helmholtz free energy. When an effective shear stress τ^* is applied, the dislocation can overcome the short-range obstacle with the activation energy of G^*.

Using the average velocity of dislocation $\bar{v}$, the following equation is derived from Eq. (16) with v_0 of the dislocation rate constant:

$$\begin{aligned}\bar{v} = \frac{\dot{\gamma}}{\rho b} &= \frac{N_0 S_0 \nu}{\rho} \exp\left(-\frac{F - \tau^* V^*}{kT}\right) \\ &= v_0 \exp\left(-\frac{F - \tau^* V^*}{kT}\right)\end{aligned} \tag{17}$$

$$\text{where } \tau^* V^* = F + kT \ln \frac{\dot{\gamma}}{\rho b v_0}. \tag{18}$$

If the experimental results were to agree with the above equation, $k \ln \frac{\dot{\gamma}}{\rho b v_0}$ must be independent of temperature, and $\tau^* V^*$ should be linear with the test temperature T. Figure 8

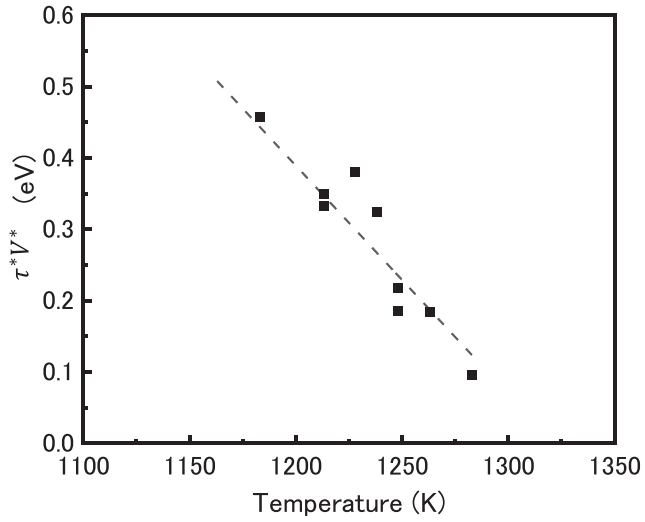

Fig. 8. Temperature dependence of τ^*V^*. Each plot coincides with the dotted line. The y-intercept of the dotted line is 4.2 ± 0.5 eV.

shows the relationship between τ^*V^* and T. From the y-intercept of Fig. 8, F is estimated to be 4.2 ± 0.5 eV. This value is close to the value obtained from Fig. 5. In other words, the Helmholtz free energy, F, and the activation energy, G^*, of the dislocation motion are nearly identical at high temperatures and low effective stresses, where the contribution of the effective stress for dislocation motion is much lower than those obtained from previous studies. In the temperature range below 1100 K, the activation enthalpy for dislocation motion is reported as 2.2 eV,[26] suggesting that the controlling process for dislocation motion in this study is not kink-pair formation and will be discussed further in the next section.

3.2.3. Contribution of self-diffusion to dislocation motion at high temperatures. Figure 9 shows the deformation mechanism map (DMM) for dislocation-free Si crystals numerically obtained by Koleshiko et al.[44] The deformation mechanism differs for the regions indicated by I to IV. In region I, the interaction between dislocations and phonons controls the plastic deformation. In region II, the plastic deformation is controlled by lattice friction (Peierls potential), while in region III it is controlled by obstacles to dislocation motion, such as forest dislocations. In region IV, creep and diffusion control the plastic deformation.[45–47] The dotted lines in Fig. 9 show the relationship between the test temperature and the flow stress for strain rates $\dot{\varepsilon}$ of 10^{-3} s^{-1} and 10^{-4} s^{-1}. As shown in Fig. 9, the plastic deformation at 1173–1373 K and $\dot{\varepsilon} = 4.7 \times 10^{-4}$ s^{-1} is controlled by lattice friction and not creep. As shown in Figs. 3–5, the values of the activation enthalpy, yield stress, and activation volume between Cz and Fz are nearly identical. This indicates that the solute oxygen does not act as an obstacle to dislocation motion and that the effects of oxygen content are nearly negligible in dislocation mobility at temperatures above 1173 K.[26] However, the activation enthalpy of ∼4.9 eV in the temperature range in the present study is much larger than 2.2 eV obtained in previous studies. An explanation for this is that the tests in the previous studies were performed in region II of the DMM.[26,27] The activation energy for self-diffusion of Si atoms is ∼4.75 eV, which is closer to the value obtained in this study.[48–50] These results suggest that the thermal activation of dislocation motion in the present study is not due to the formation of kink pair but is assisted by diffusion.

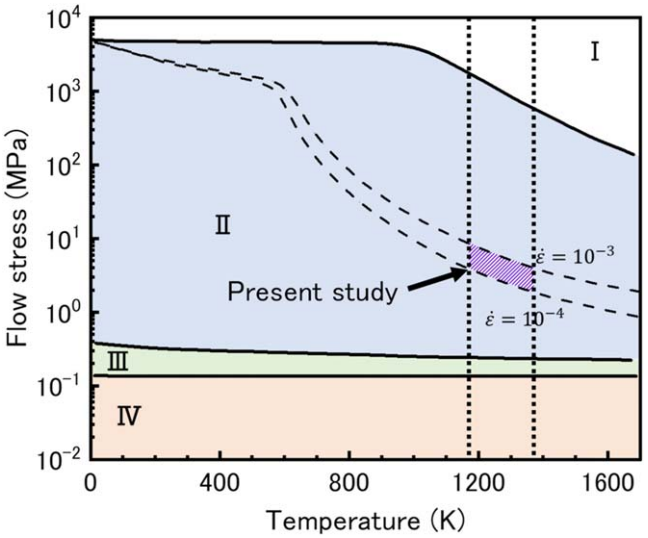

Fig. 9. (Color online) Deformation mechanism map of dislocation-free Si.[44] The deformation mechanism differs for the regions indicated by I to IV. The experimental conditions in the present study are shown as the shaded area in the figure.

The large activation enthalpy for plastic deformation at high temperatures was also reported by Farber et al.[51] Here, we discuss the diffusion length of Si self-diffusion and use this to validate its role in the dislocation motion using the dislocation velocity obtained in previous studies. The distance x over which a dislocation moves during time t can be obtained from Eq. (11) as follows:

$$x = vt = B_0 t(\tau/\tau_0)^m \exp(-H^*/kT). \tag{19}$$

The specific values of each of these constants, as reported in the literature, are $B_0 = 10^4$ m s^{-1} · MPa, $\tau_0 = 1$ MPa, $m = 1.0$ and $H^* = 2.2$ eV.[26,52] The variable τ in Eq. (19) is the CRSS. The diffusion length r can be expressed as follows:

$$r = \sqrt{Dt} = \sqrt{D_0 t \exp(-E/kT)}, \tag{20}$$

where D is the diffusion coefficient, D_0 is the pre-factor, and E is the activation energy for self-diffusion; $D_0 = 1.5 \times 10^7$ m^2 s^{-1} and $E = 4.75$ eV.[48–50]

Figures 10(a)–10(c) show the relationship between x, r, and b and the diffusion time t at 1000 K, 1130 K, and 1300 K, respectively, calculated using Eqs. (19) and (20). The blue and red lines indicate the dislocation motion distance and diffusion length over time, respectively. The dotted line shows the magnitude of the Burgers vector. Times when the dislocation motion distance and diffusion length coincide with the magnitude of the Burgers vector b are given as t_x and t_D, respectively. Hence, b/t_x is the velocity of the dislocation, and b/t_D is the velocity at which the atom diffuses over a Burgers vector length. As shown in Fig. 10, the relationship between t_x and t_D is $t_x < t_D$ at 1000 K, $t_x = t_D$ at 1130 K, and $t_x > t_D$ at 1300 K. In other words, at 1000 K, the diffusion rate is slow relative to the dislocation velocity, whereas the dislocation velocity and diffusion rate almost coincide at 1130 K. At temperatures higher than 1130 K, the self-diffusion rate is faster than the dislocation velocity, indicating that the diffusing atoms (or vacancies) can follow

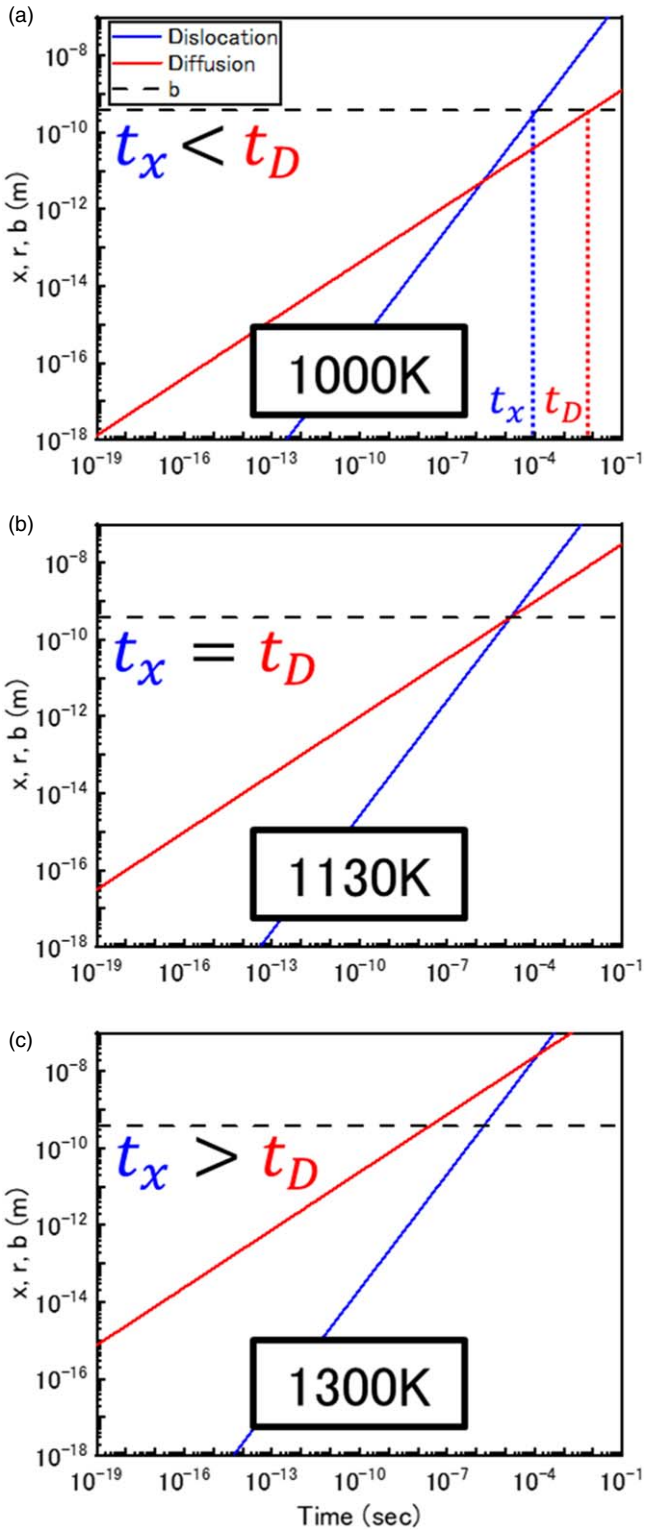

Fig. 10. (Color online) Relationship between the distance of the dislocation motion, x, and the diffusion length, r, versus time at test temperatures of (a) 1000 K, (b) 1130 K, (c) 1300 K. The dotted lines show the length of the Burgers vector of b. t_x is the time when a dislocation moves the distance of b, while t_D is the time when a Si atom diffuses the distance of b.

dislocation motion. In addition, the dislocation velocity at 1130 K obtained from Eqs. (19) and (20) is estimated to be 56 μm s^{-1}, which is a reasonable value.[26,52] Thus, the high activation energy of the dislocation motion obtained experimentally at temperatures above 1130 K suggests that self-diffusion of atoms plays an important role in the dislocation motion.

Thus, we consider the following hypotheses for the thermal activation of dislocation motion in Si. First, at low temperatures below 1130 K, where self-diffusion has no direct effect on the dislocation motion, the main barrier to dislocation motion is the Peierls potential. The formation and glide of kink-pair govern the dislocation rate here. By contrast, dislocations move like recombined atoms assisted by self-diffusion at temperatures above 1130 K, where the diffusion length is greater, In fact, Nishino et al. observed that the angular dislocation lines became smooth when Si was annealed above 1173 K.[53] Figure 11 shows an example of the case of an edge dislocation containing a row of vacancies along the dislocation line. Here, the dislocation moves with the row of vacancies in a manner similar to diffusion. Even though the dislocation motion appears similar to that of a dislocation glide, the thermally activated dislocation is unable to overcome the Peierls potential. If self-diffusion assists dislocation motion, dislocations can overcome the Peierls potential to a certain extent. The very large activation volume can be explained by assuming that dislocation segments of a certain length move over the Peierls potential without forming a kink-pair. In other words, the Peierls potential is still the main obstacle controlling the dislocation velocity even at extremely high temperatures such as those in this experiment; however, thermal activation of dislocation motion is different from that of kink pair formation, suggesting that self-diffusion plays an important role in dislocation motion, as suggested by Farber–Nikitenko.[51]

4. Conclusions

Tensile tests and strain rate change tests of Si single crystals were conducted at 1123–1373 K, and the following results were obtained:

(1) The yield stress showed a remarkable temperature dependence, and it decreased with increasing test temperature. However, above 1323 K, the yield stress did not change with a further increase in the test temperature.
(2) The values of the yield stress and activation enthalpy were not significantly different between the Cz and Fz crystals, indicating that the solute oxygen is not the obstacle for dislocation motion. The thermal activation process is identical between them at the strain rate and test temperature range used in this study.
(3) The measured activation volume and energy were found to be much larger at higher temperatures than those obtained at lower temperatures, indicating that the

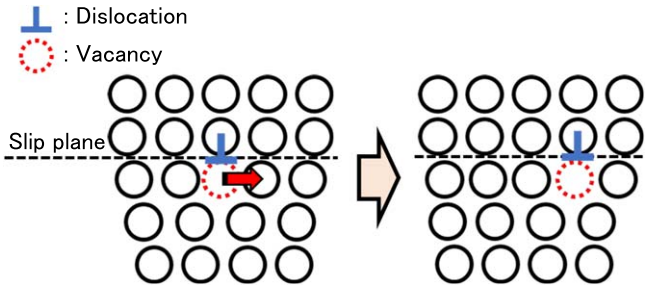

Fig. 11. (Color online) Schematic diagram of the edge dislocation gliding with the silicon atoms in the diffusion process.

thermal activation process of dislocation glide is different at lower and higher temperatures.

(4) The rate-limiting process for dislocation motion at lower temperatures is the formation and movement of kink pairs, whereas at higher temperatures, self-diffusion is the rate-limiting process for dislocation motion.

Acknowledgments

This work was partly supported by a Grant-in-Aid for Scientific Research (A) (JP18H03848).

ORCID iDs

Tubasa Suzuki https://orcid.org/0000-0003-4508-8459
Masaki Tanaka https://orcid.org/0000-0002-4982-257X

1) H. Shimizu, S. Isomae, K. Minowa, T. Satoh, and T. Suzuki, J. Electrochem. Soc. **145**, 2523 (1998).
2) S. M. Hu, J. Appl. Phys. **40**, 4413 (1969).
3) J. Bloem and A. H. Goemans, J. Appl. Phys. **43**, 1281 (1972).
4) S. M. Hu, J. Vac. Sci. Technol. **14**, 17 (1977).
5) H. Alexander, R. Labusch, and W. Sander, Solid State Commun. **3**, 357 (1955).
6) C. Auth et al., Proc. IEEE Int. Electron Devices Meeting (IEDM), 2017, p. 1, 10.1109/IEDM.2017.8268472.
7) *The International Technology Roadmap for Semiconductors: Executive Summary* (Semiconductor Industry Association, Washington, DC, 2015) Vol. 39.
8) N. Tsuchiya, O. Fuji, K. Umezawa, M. Iwase, and Y. Ushiku, IEEE Trans. Semiconductor Manuf. **18**, 19 (2005).
9) K. Ishimaru et al., Dig. 1997 Symp. VLSI Technology, Kyoto, Japan, 1997, p. 123.
10) H. Ohta, H. Miura, and M. Kitano, J. Soc. Mater. Sci. Jpn. **45**, 1322 (1996).
11) M. Omri, C. Tete, J.-P. Michel, and A. George, Philos. Mag. A **55**, 601 (1987).
12) I. Yonenaga and K. Sumino, Phys. Status Solidi A **50**, 685 (1978).
13) A. Giannattasio, S. Senkader, R. J. Falster, and P. R. Wilshaw, Physica B **340-342**, 996 (2003).
14) I. Yonenaga, J. Electrochem. Soc. **143**, L176 (1996).
15) J. R. Patel and A. R. Chaudhuri, J. Appl. Phys. **34**, 2788 (1963).
16) J. Fujise, B. Ko, T. Ono, and M. Tanaka, Jpn. J. Appl. Phys. **57**, 035501 (2018).
17) J. Fujise, B. Ko, T. Ono, and M. Tanaka, ECS J. Solid State Sci. Technol. **9**, 055012 (2020).
18) T. Suzuki, M. Tanaka, T. Morikawa, Y. Okuyama, J. Fujise, and T. Ono, Mater. Trans. **62**, 975 (2021).
19) R. Falster, M. Pagani, D. Gambaro, M. Cornara, M. Olmo, G. Ferrero, P. Pichler, and M. Jacob, Solid State Phenom. **57**, 58 (1997).
20) R. Falster, V. V. Voronkov, and F. Quast, Phys. Status Solidi (b) **222**, 219 (2000).
21) M. Pagani, R. J. Falster, G. R. Fisher, G. C. Ferrero, and M. Olmo, Appl. Phys. Lett. **70**, 1572 (1997).
22) M. Akatsuka, M. Okui, N. Morimoto, and K. Sueoka, Jpn. J. Appl. Phys. **40**, 3055 (2001).
23) K. Araki, S. Maeda, T. Senda, H. Sudo, H. Saito, and K. Izunome, ECS J. Solid State Sci. Technol. **2**, 66 (2013).
24) K. Sumino and I. Yonenaga, Jpn. J. Appl. Phys. **20**, L685 (1981).
25) M. Kato, *Introduction to the Theory of Dislocations* (Shokabo, Tokyo, 1999) p. 100.
26) M. Imai and K. Sumino, Philos. Mag. A **47**, 599 (1983).
27) V. N. Erofeev and V. I. Nikitenko, Sov. Phys. JETP **33**, 963 (1971).
28) T. Taoka, S. Takeuchi, and E. Furubayashi, J. Phys. Soc. Jpn. **19**, 701 (1964).
29) S. Takeuchi, E. Furubayashi, and T. Taoka, Acta Metall **15**, 1179 (1967).
30) T. Suzuki and S. Takeuchi, Mater. Japan **40-2**, 164 (2001).
31) C. R. Weinberger, B. L. Boyce, and C. C. Battaile, Int. Mater. Rev. **58-5**, 296 (2013).
32) R. Gröger, A. G. Bailey, and V. Vitek, Acta Mater. **56**, 5401 (2008).
33) W. Cai, V. V. Bulatov, J. Chang, and J. Li, *Dislocations in Solids* (North Holland, Amsterdam, 2004) Vol. 12, p. 1.
34) T. Imura, K. Noda, H. Matsui, and H. Saka, *Dislocation in Solids* (Univ. Tokyo Press, Tokyo, 1985) p. 287.
35) K. Edogawa, T. Suzuki, and S. Takeuchi, Phys. Rev. B **55**, 6180 (1997).
36) W. G. Johnston, J. Appl. Phys. **33**, 2716 (1962).
37) W. C. Dash, *Dislocations and Mechanical Properties of Crystals* (Wiley, New York, 1957) p. 57.
38) P. Haasen, J. de Phys. **40**, 111 (1978).
39) P. B. Hirsch, J. de Phys. **40**, 117 (1978).
40) R. Jones, J. de Phys. **44**, 33 (1983).
41) Y. Yamashita, K. Maeda, K. Fujita, N. Usami, K. Suzuki, S. Fukatsu, Y. Mera, and Y. Shiraki, Phil. Mag. Letter **67**, 165 (1993).
42) A. Seeger, Phil. Mag. **1**, 651 (1956).
43) J. Lothe and J. P. Hirth, Phys. Rev. **115**, 543 (1959).
44) V. M. Koleshko and I. V. Kiryushin, Phys. Status Solidi (a) **109**, 161 (1988).
45) J. D. Eshelby, Proc. R. Soc. A **197**, 396 (1949).
46) G. Leibfried, Z. Phys. **127**, 344 (1950).
47) W. P. Mason, J. Acoust. Soc. Am. **32**, 458 (1960).
48) G. M. Hood and J. N. Sherwood, J. Chim. Phys. **63**, 121 (1966).
49) A. Berne, G. Boato, and M. M. De Paz, Nuovo Cimento B **46**, 182 (1966).
50) E. H. C. Parker, H. R. Glyde, and B. L. Smith, Phys. Rev. **176**, 1107 (1968).
51) B. Ya. Farber and V. I. Nikitenko, Phys. Status Solidi A **73**, K141 (1982).
52) I. Yonenaga and J. M. Sci, Mater. Electron **10**, 329 (1999).
53) Y. Nishino, H. Saka, and T. Imamura, J. Mater. Sci. **19**, 245 (1984).